Clickable Iron Oxide NPs Based on Catechol Derived Ligands: Synthesis and Characterization.

Esther Pozo-Torres[a,‡], Carlos Caro[a,b,‡], Ashish Avasthi[b], Jose María Páez-Muñoz, María Luisa García-Martín[b,c,*], Inmaculada Fernández[a,*], Manuel Pernia Leal[a,*].

[a]Departamento de Química Orgánica y Farmacéutica, Facultad de Farmacia, Universidad de Sevilla, 41012 Seville (Spain)

[b]BIONAND, Andalusian Centre for Nanomedicine and Biotechnology, C/ Severo Ochoa, 35, Junta de Andalucía, Universidad de Málaga, 29590 Málaga, Spain

[c]Networking Research Center on Bioengineering, Biomaterials and Nanomedicine, CIBER-BBN, 29590 Málaga, Spain

[‡]Esther Pozo and Carlos Caro contributed equally to this work.

* email: mpernia@us.es; inmaff@us.es; mlgarcia@bionand.es

Abstract

Clickable magnetic nanoparticles have attracted great attention as potential nanoplatforms for biomedical applications because of the high functionalization efficiency of their surfaces with biomolecules, which facilitates their bio-compatibilization. However, the design and synthesis of clickable NPs is still challenging because of the complexity of the chemistry on the magnetic NP surface, thus being in high-demand robust methods that improve the ligand synthesis and the transfer of magnetic NPs in physiological media. In this work, we developed a versatile and enhanced synthetic route to fabricate potentially clickable IONPs with interest in nanomedicine. Catechol anchor ligands with different stereo-electronic features were

synthetized from a hetero bi-functional PEG spacer backbone. The resulting catechol ligands transferred in good yields and high stability to magnetic NPs by an improved energetic ligand exchange method that combines sonication and high temperature. The azido functionalized IONPs exhibited excellent characteristics as T_2 MRI contrast agents with low cytotoxicity, making these clickable magnetic NPs promising precursors for nanomedicines.

Introduction

One of the main challenges in the nanomedicine field is the development of robust methods to properly transfer functionalized magnetic nanoparticles in physiological media.[1-4] The as-prepared magnetic nanoparticles are mostly not soluble in aqueous solution or they do not present the minimal requirements for *in vivo* applications, such as low toxicity, high colloidal stability and non-alteration of their initial properties.[5-8] Hence, the chemistry on the magnetic nanoparticle surface is becoming a tough task, the functionalization process being crucial for the improvement in the design and synthesis of nanomedicines.[9-11] Among the different approaches, ligand exchange is the most reliable method since the synthesized ligand could be easily characterized by NMR and FTIR techniques before the interaction with the magnetic NPs.[12-17] However, it is not always possible to prepare the required final ligand previous to the functionalization.[18] This is likely due to steric interactions between the ligand molecules, an unbalanced hydrophilicity-hydrophobicity ratio, cross-linking or degradation problems during the process. Therefore, the incorporation of biomolecules, drugs or other functionalities in the ligand molecule has to be performed after the ligand exchange on the NP surface.[19-21] A model ligand molecule should present hetero-bi functionality, with a specific reactive group on one side of the ligand and a strong anchor group on the other side.

The specific reactive group in the ligand attached to the NP surface will be exposed to the medium allowing other desired molecules to be specifically conjugated without altering the properties of the NPs and minimizing possible side reactions. The so-called Click chemistry, a term introduced in 2001 by K. B. Sharpless, includes a type of organic reaction characterized by high yield, mild reaction conditions, regioselectivity and non-specific couplings even in the presence of other functional groups.[22] The use of this Click concept, and in particular the Cu(I)-catalyzed 1,3-dipolar cycloaddition of azides and alkynes, has attracted the interest in the nanomedicine field because of the ease to functionalize the surface of magnetic NPs with biomolecules such as drugs, proteins or peptides, for instance.[23-28] Catechol-based ligands are especially interesting in material chemistry due to their ability to functionalize and stabilize magnetic nanoparticles in physiological media.[16, 24, 29] In particular, catechol-derived anchors have been shown to interact strongly with the surface of iron oxide nanoparticles (IONPs) through the phenolic hydroxyl groups.[16, 30] The bi-dentate catechol unit reacts with the Fe cation likely forming a quite stable 5-membered ring complex, in the same manner as the iron-catecholate complex ($[Fe(cat)_3]^{3-}$) obtained in solution.[31] The thorough characterization of the NP-catechol bonding by physicochemical techniques has demonstrated that the NPs remain unaltered, maintaining their original magnetic properties. Herein, we describe a rational design to prepare functional clickable magnetic NPs from different catechol-derived ligands. These ligands present a tuneable spacer derived from polyethylene glycol (PEG) (200 or 1500 Da) with an azide group as a clickable point at one end and a catechol anchor at the other, such as caffeic acid (CA), dihydro caffeic acid (DHCA) or gallic acid (GA). The stereo-electronic features of these different catechols determine both the coupling effectiveness with the PEG spacers for the synthesis of the corresponding ligands, and their affinities towards iron

oxide NPs. Furthermore, an improved efficient ligand exchange procedure has been developed that increases the transference of magnetic NPs into the water phase without altering their properties. An extensive *in vitro* characterization of the resulting functionalized NPs by different physicochemical and cytotoxic analysis confirmed the potential of these functional clickable NPs for biomedical applications.

Results and Discussion

Synthesis of catechol derived TEG-N_3 ligands and functionalization of NPs.

The synthesis of clickable PEGylated catechol ligands was performed by coupling the corresponding catechol acid moiety with the previously prepared hetero bi-functional clickable PEG spacer **(Figure 1)**. In these studies, tetraethylene glycol (TEG, a low molecular weight PEG) was chosen as the spacer backbone. The hetero bi-functional TEG spacer (**9**) was synthesized following the protocol reported by Mattoussi and col.[32] The subsequent amide coupling between the amino-TEG-azide spacer **9** and the corresponding catechol acids rendered pure CA-TEG-N_3 (**1**) and DHCA-TEG-N_3 (**2**) ligands with 26% and 48% yield, respectively **(Scheme 1)**. Unfortunately, the GA-TEG-N_3 (**3**) ligand could not be purified by column chromatography due to the high polarity of the three phenolic OH groups present in the catechol moiety. Indeed, a similar or lower yield is expected for the synthesis of this ligand compared to that obtained with the caffeic derived ligand, due to the lower reactivity of the carboxylic acid conjugated with the aromatic ring. The ligand exchange onto the iron oxide NP surface of the catechol derived TEG ligands was performed following our previously reported procedure.[10] The gentle shaking of a mixture containing 10 nm IONPs (**Figure S19**), the corresponding catechol derived azido TEG ligands and a base, did not lead to water soluble NPs. This could be due to the poor hydrophilic behaviour of the TEG

ligands, thus being necessary to increase it by using a higher molecular weight PEG 1500 Da spacer (named just PEG from now on).

Synthesis of catechol derived PEG-N_3 ligands and functionalization of NPs.

The hetero bi-functional PEG spacer was synthesized using a protocol different from that described above for the TEG spacer, since in this case the di-azide PEG derivative is soluble in both organic and water phases. Therefore, the design of the hetero bi-functional PEG spacer was slightly changed to an alcohol-azido derivative instead of the original amino-azido one, being synthesized in only two steps with 70% yield (**Scheme 2**).[33] The esterification of the catechol acid moieties with the alcohol-azido PEG spacer (**12**) gave the desired ligands **4-6** (**Scheme 2**), which were used in the NP functionalization process without previous purification because the very similar polarity of both the starting alcohol and the obtained ester derivatives did not allow their separation by column chromatography (see Supporting Information). Indeed, the removal of unreacted hetero bi-functional PEG spacer was done by a dialysis process.[10, 11, 17]

Successfully, the ligand exchange with the catechol derived PEG ligands transferred the magnetic NPs to the water phase. The elongation of the ethylene chain in the catechol derived ligands assisted the solubilization of magnetic NPs in aqueous solution. ICP-MS was performed before and after ligand exchange to accurately determine the total amount of magnetic NPs transferred to the aqueous phase. The percentages of ligand exchange for the catechol derived PEG azides were 11% and 3% for the CA-PEG-N_3 (**4**) and DHCA-PEG-N_3 (**5**) ligands respectively and 18% for the GA-PEG-N_3 (**6**) ligand (**Figure 2a**). Interestingly, despite the low yield in the synthesis of the ligand **6**, it rendered the highest exchange of magnetic NPs. The hydroxyl groups in the gallate-

derived ligand are more acidic than the hydroxyl groups in the DHCA due to the conjugation with the carbonyl group, as discussed above. Although similar results were expected for the ligand **4**, the percentage of ligand exchange resulted 1.6 times lower than that obtained with the GA-PEG-N_3 ligand but 4 times higher than that of the DHCA-PEG-N_3 ligand. In general, the low transfer of magnetic NPs to the water phase through a gentle ligand exchange with the catechol derivatives could be due to the high pH value of the medium. It has been reported that the ligand exchange procedure on magnetic NPs depends on the charges of both the oleic acid capping NPs and the anchoring ligands, being optimal when the magnetic NP surface are positively charged and the ligands have negative charges.[34] The as-prepared magnetic NPs are reported to exhibit positive surface charges at pH below 6.8. However, the catechols GA, CA and DHCA derivatives present high pKa values (above 9), which makes it not possible to get a suitable pH value that compromises both charges. The ligand exchange procedure has been tested without success at more acidic pH values (from 6 to 8) than the one already used (pH~9). Then, a more energetic exchange procedure was performed to force the catechol ligands to replace the oleic acid molecules and chemically interact with the magnetic NP surface. The mixture of catechol ligands, magnetic NPs and base was previously sonicated for 1 h, followed by incubation at 50 ºC for 4 h. After that, the mixture was separated gently in a separation funnel as described in the Experimental Section. This new procedure resulted in a higher transfer of magnetic NPs to the aqueous phase, as shown **Figure 2**. The GA-PEG-N_3 and CA-PEG-N_3 ligands presented the highest yield values (51% and 41%, respectively), as expected considering their similar stereo-electronic features compared to the DHCA-PEG-N_3 ligand (38%). TEM images showed that the resulting GA-PEG-N_3-NPs were well dispersed on the grid with the absence of aggregates (**Figure 3**). In contrast, the TEM images of the other two

catechols derived NPs showed the presence of the functionalized NPs together with either small aggregates, in the case of functionalization with the CA-PEG-N_3, or big aggregates, in the case of functionalization with the DHCA-PEG-N_3. Interestingly, the ligand **5** self-organized in a liposome-like structure of ca. 200 nm in size covered with magnetic NPs (**Figure 3**). In order to determine the capacity of the catechol derived PEG ligands to form supramolecular structures by themselves without the presence of any template (as could be the NPs), the synthesis of liposomes from the different catechol PEG ligands was carried out following standard reported protocols (see Supporting Information).[26] The resulting TEM images showed that only DHCA-PEG-N_3 ligand was able to self-organize in supramolecular structures with diameters around 81 nm and 141 by TEM and DLS respectively (**Figure S18**).

Synthesis of catechol derived PEG-OH ligands and functionalization of NPs.

Catechol derived PEG ligands terminated in hydroxyl groups were synthesized to compare the effect of the azide groups in the ligand exchange on magnetic NPs (**Scheme 3**). Therefore, all these ligands successfully transferred the magnetic NPs by using the most energetic exchange procedure, resulting in yields in a range of 28-61% (**Figure 2**). It should be noted that these yields are significantly higher than those obtained with the previously described gentle method (between 6.5-28%), indicating that this new ligand exchange procedure is very robust and efficient. TEM images of the functionalized catechol-based NPs showed the presence of monodispersed NPs without the formation of aggregates (**Figure 3**). None of these ligands generated supramolecular structures under these conditions. These results demonstrated the important influence of the nature of the terminal group of the ligand, alcohol or azide, on the functionalization of NPs as well as on the formation of supramolecular structures in the case of the DHCA-PEG.

The colloidal stability of catechol PEG azide and OH functionalized NPs was analyzed in different media at different times (**Figure 2** and **Figure S20**). It is well known that the size of NPs depends on several factors, such as salt concentration and presence of proteins.[30, 35, 36] Therefore, the colloidal stability of functionalized NPs was studied in water, PBS buffer and Fetal Bovine Serum (FBS). In general, the catechol PEG NPs did not exhibit remarkable differences over time, except for CA-PEG-N_3-NPs and DHCA-PEG-N_3-NPs, which formed aggregates during their functionalization, as shown in the TEM images (**Figure 3**). Small variations of 1-2 nm in their hydrodynamic (HD) sizes in water and PBS buffer were observed after one week (**Figure 2**). In contrast, greater variations were observed in FBS, around 4-8 nm for the OH functionalized NPs and 14 nm for the GA-PEG-N_3-NPs. This substantial difference in the HD sizes is likely due to the higher number of interactions of the azide PEG ligands with proteins as compared to the hydroxyl PEG ligands.

FTIR analysis was performed to determine the presence of the ligands onto the NP surface. As can be observed in **Figure 4, Figure S21, Figure S22 and Table S1**, the main peaks of the ligands correspond to the PEGylated part. In the case of catechol PEG-OH ligands, the main peaks in the spectrum can be assigned to C-H stretching (3000-2700 cm^{-1}), aromatic C=C stretching (1600-1400 cm^{-1}), C–H bending (1466 cm^{-1}, 1359 cm^{-1} and 1341 cm^{-1}), anti-symmetric stretching (1307 cm^{-1}), C–O stretching (1268 cm^{-1}, 1238 cm^{-1}), C–O–C stretching (1092 cm^{-1}), CH out-of-plane bending (942 cm^{-1}) and aromatic CH out-of-plane bending (900-675 cm^{-1}). The catechol PEG-N_3 ligands showed the same main peaks described above with the appearance of a peak at 2105 cm^{-1} that can be assigned to a N=N=N stretch vibration.

To evaluate the potential of these functionalized magnetic NPs as Magnetic Resonance Imaging contrast agents (CA), r_2 relaxivities were measured at low and high magnetic

fields (**Figures S24-S25** and **Figure 5**). As in the colloidal stability studies, all magnetic NPs functionalized with catechol derived PEG-OH ligands (**13-15**) showed similar relaxivities, with r_2 values ranging from 49.7 to 63.6 $mM^{-1}\cdot s^{-1}$ at low magnetic field and from 128.6 to 133.3 $mM^{-1}\cdot s^{-1}$ at high magnetic field (**Figure S24**). The similarity of the r_2 values can be justified by the fact that they all have the same magnetic core. The GA-PEG-N_3-NPs showed the highest r_2 values, 72.6 and 167.9 $mM^{-1}\cdot s^{-1}$ at low and high magnetic fields, respectively, and the catechols CA- and DHCA-PEG-N_3-NPs showed the lowest r_2 values, 31.2 and 39 $mM^{-1}\cdot s^{-1}$ at low magnetic field and 28 and 71 $mM^{-1}\cdot s^{-1}$ at high magnetic field, respectively (**Figure S25**). An unexpected decrease in the r_2 value at high magnetic field was observed for the DHCA-PEG-N_3-NPs, which can be attributed to the precipitation of the NPs during the time course of the experiment. Regarding longitudinal relaxivity (r_1), all the catechol derived NPs showed very low r_1 values at both magnetic fields, indicating that these NPs behave exclusively as T_2 contrast agents.

Cu(I)-catalyzed 1,3-dipolar cycloaddition on the magnetic NP surface.

To confirm the possibility of incorporating different molecules on the NP surface by a click reaction, we performed a reaction between the NP-GA-PEG-N_3 and propargylamine as an alkyne molecule model with copper sulfate and sodium ascorbate as catalysts. After purification of the resulting triazole-NPs through centrifugal filters with molecular weight cut-off of 100 kDa, the triazole-NPs were analyzed by FTIR spectroscopy. As shown in **Figure 6**, the peak at 2100 cm^{-1} corresponding to N=N=N stretching decreases in intensity after the click reaction thus indicating the transformation of an important number of azides into triazole groups onto the NPs surface. Moreover, three new peaks corresponding to the amine group appeared around 3400 cm^{-1} (N-H stretching), 1600 cm^{-1} (N-H bending) and 1350 cm^{-1} (C-N stretching).

These results confirm the incorporation of propargylamine molecules to the surface of magnetic NPs by a click reaction.

Finally, an essential feature of the IONPs functionalized for biomedical applications is the biocompatibility.[37-39] This is crucial in the case of the catechol derived-NPs since some phenolic compounds showed cytotoxic effects by oxidative damage to biomolecules, such as DNA and proteins.[40, 41] The cellular biocompatibility of the catechol derived NPs was assessed in cell culture using human foreskin fibroblasts HFF-1. Cultured cells were exposed to increasing concentrations of functionalized NPs from 0.1 μg/mL to 100 μg/mL (**Figures S26-S31** and **Figure 7**). An exhaustive evaluation of cytotoxicity was performed, including cell morphology and mitochondrial activity assays, as well as "live-dead" experiments (**Figures S26-S31**). The gallate and caffeate derived-NPs did not show any adverse effect, indicating that these four NPs are promising candidates for biomedical applications (**Figure 7**). On the other hand, the DHCA-PEG-OH-NPs induced a significant decrease in mitochondrial activity (< 80%) at a concentration of 100 μg/mL ($p<0.05$), indicating that these NPs affect the metabolism of fibroblasts, but no effect was observed on the morphology or cell viability (**Figure 7**). In the case of DHCA-PEG-N_3-NPs, it can be observed the appearance of cells in apoptosis or even death at a concentration of 100 μg/mL (**Figure 7h**). The "live-dead" assay showed a decrease of the total number of cells at a NPs concentration of 10 μg/mL ($p<0.05$), and an increase of death cells for concentrations of 100 μg/mL ($p<0.05$). These results are in good agreement with the MTT experiments that showed a decrease below 90% of normal mitochondrial activity at a concentration of 10 μg/mL, reaching even lower mitochondrial activity (around 60%) at a concentration of 100 μg/mL ($p<0.05$) (**Figure 7j**).

Conclusions

In summary, we have reported the synthesis of clickable iron oxide NPs as potential MRI contrast agents. The synthetic design is based on a modular and versatile hetero bi-functional PEG spacer with an azide group and a catechol moiety at each end. Three catechol derivatives with different stereo-electronic features have been evaluated as efficient anchors for the functionalization of iron oxide NP surface. Catechol ligands with high molecular weight, above 1500 Da, were able to transfer IONPs in aqueous media. An improved energetic ligand exchange method, which combines sonication and high temperature, boosted the exchange of the capping agents for the catechol derived molecules on the NP surface. The gallate and caffeate derived azido PEG ligands transferred higher number of IONPs in comparison with DHCA derivates. In contrast, the DHCA-PEG-azido ligands self-organized in a liposome-like structure of 200 nm. The gallate PEG IONPs showed the highest transversal relaxivities, r2, at both high and low magnetic fields. The catechols CA and DHCA azido-NPs showed quite low r2 values at high magnetic field due to the precipitation of small aggregates formed during ligand exchange. The azido functionalized iron oxide NPs did not show any adverse effects in cultured cells. The combination of these results supports the great potential of the gallate PEG azido IONPs as clickable nanoparticle for diagnostic and/or therapeutic applications.

Experimental Section

General Method for the incorporation of PEG spacers to catechols: To a solution of a PEG spacer (1 mmol), EDC (1.5 mmol), HOBt (1.2 mmol) and DIPEA (3 mmol) in DMF (10 mL) in a round-bottom flask under argon atmosphere and at 0ºC was added dropwise a solution of the catechol (1 mmol) in DMF (10 mL). The mixture was stirred overnight at room temperature. DMF was evaporated and it was diluted with CH_2Cl_2 (250 mL) and washed with 1M HCl (50 mL), saturated aqueous $NaHCO_3$ solution (50

mL) and brine (50 mL), and dried over Na_2SO_4. Solvents were rota-evaporated to yield the crude product. The crude was purified by silica gel column chromatography eluting with dichloromethane/methanol.

Hetero bi-functional spacer azido-PEG-OH (12): To a solution of polyethylene glycol (Mw = 1500 g/mol) (40 g, 26.7 mmol), Et_3N (5 mL, 32 mmol) and THF (200 mL) was cooled to 0ºC. To this mixture was added dropwise methanesulfonyl chloride (2.06 mL, 26.7 mmol). The reaction mixture was then allowed to warm to room temperature and stirred vigorously overnight. The solution was diluted with CH_2Cl_2 (250 mL) and washed with saturated $NaHCO_3$ (50 mL) and brine (50 mL). The organic solution was dried over Na_2SO_4, and the solvents were removed under vacuum. The crude was carried out to the next step without any further purification.

A mixture of mesylated compound (26.7 mmol) and sodium azide (2.2 g, 40 mmol) in ethanol (100 mL) was heated at reflux overnight, cooled to room temperature and concentrated in the rota-evaporator. The residue was diluted with CH_2Cl_2 (250 mL), washed with brine (50 mL), and dried over Na_2SO_4. Solvent was removed under vacuum to yield the crude product, which was purified by flash column chromatography, eluting with CH_2Cl_2/MeOH (20:1) to give **15** as a white solid (13 g, 65%). ^{1}H NMR (300 MHz, $CDCl_3$) δ: 3.75-3.60 (m CH_2-PEG, -OH), 3.42-3.37 (m, 2H), 2.63 (t, *J* = 5.9 Hz, 2H).

General Methods to functionalize magnetic NPs: Two different ligand exchange procedures have been tested:

Protocol 1*:* the functionalization of the magnetic NPs was performed following the previously protocol published.[10] Briefly, in a separating funnel was added a solution of magnetic nanoparticles in toluene (1 mL, 10 g of Fe/L), a solution of the corresponding ligand in chloroform (1 mL, 0.1 mM) and trimethylamine (50 μL). The mixture was

shaked gently and it was diluted with toluene (5 mL), milli-Q water (5 mL) and acetone (10 mL). Then, the mixture was shaken and the aqueous phase was collected in a round-bottom flask and the residual organic solvents were rota-evaporated. The functionalized magnetic NPs were purified in centrifuge filters (100 kDa cut-off) at 450 rcf until the filtrate was complete cleared. Finally, the magnetic NPs was diluted in the corresponding medium and centrifuged at 150 rcf for 5 min and also, it was placed onto a permanent magnet (0.6 T) for 5 min to remove the big aggregates.

Protocol 2*:* In a glass vial a mixture of a toluene solution of magnetic nanoparticles (1 mL, 10 g of Fe /L), a chloroform solution of the corresponding ligand (1 mL, 0.1 mM) and trimethylamine (50 μL) was ultrasonicated for 1 h. Next, the mixture was heated to 50 ºC for 4 h. Then, the mixture was transferred into a separating funnel and it was followed the same protocol described above in the protocol 1.

Method for the Cu(I)-catalyzed 1,3-dipolar cycloaddition on the NP surface.

To a suspension of GA-PEG-N_3-NPs (~0.3 mmol of azide groups calculated by TGA (Figure S23)) and propargylamine (0.3 mmol) in H_2O (1 mL) was added a solution of $CuSO_4 \cdot 5H_2O$ (0.045 mmol) and sodium ascorbate (0.13 mmol) in H_2O (1 mL). The mixture was magnetically stirred at 25 ºC for 72 h. Then, the NPs were purified through a centrifugal filter (MWCO: 100 kDa) at 150 rcf. This step was repeated until a clear solution was obtained. Finally, the triazole-NPs were re-suspended in water.

Transmission Electron Microscopy (TEM): TEM images were obtained on a FEI Tecnai G2 Twin microscope operated at an accelerating voltage of 100 kV. TEM samples were prepared by dropping a solution of the corresponding magnetic nanoparticles at ~1 g/L of Fe on a carbon-coated copper grid and letting the solvent evaporate. The diameters were calculated on an average of hundred NPs measured.

Dynamic Light Scattering (DLS): The size distribution measurements of the magnetic NPs were performed on a Zetasizer Nano ZS90 (Malvern, USA). The nanoparticles were dispersed in the corresponding medium at a concentration of 50 mg/L of Fe. The measurements were done on a cell type: ZEN0118-low volume disposable sizing cuvette, setting 2.420 as refractive index with 173º Backscatter (NIBS default) as angle of detection. The measurement duration was set as automatic and three as the number of measurements. As analysis model the general purpose (normal resolution) was chosen. For the size distribution measurement, the number mean was selected.

Fourier Transform Infra-Red Spectroscopy (FTIR). FTIR spectra were recorded with a FTIR-4100 Jasco using a single reflection ATR accessory (MIRacle ATR, PIKE Technologies) coupled to a liquid nitrogen cooled mercury cadmium telluride (MCT) detector. All spectra were recorded in the 4000 to 800 cm^{-1} range at 4 cm^{-1} resolution and accumulating 50 scans. Ligands were deposited and magnetic NPs were prepared by dropcasting of a highly concentrated NP solution onto a microscope slide.

Thermogravimetric analysis (TGA). TGA was performed on a Mettler-Toledo system (TGA/DSC 1) in the temperature range 30–800 ℃ with a heating rate of a 10 ℃/min under N_2 flow (50 mL/min). The percentage of the organic layer on the magnetic NP was quantified by thermo-gravimetric analysis, giving values of 50% for the catechol PEG-OH and 70%, 75% and 60% for the catechol CA-, DHCA and GA- PEG-N_3 NPs, respectively.

In vitro **longitudinal and transversal relaxivities (r_1 and r_2):** r_1 and r_2 relaxivities were calculated at two different magnetic fields, 1.5 T (Bruker Minispec) and 9.4 T (Bruker Biospec) using concentrations of NPs between 0.5 and 0.031 mM of Fe in physiological conditions, at 37 ºC. T_1 was determined either using inversion-recovery or saturation recovery sequences and T_2 was determined using the Carl-Purcell-Meiboom-

Gill (CPMG) sequence. r_1 and r_2 relaxivities at high field (9.4 T) were measured on a Bruker Biospec MRI system equipped with 400 mT m^{-1} field gradients and a 40 mm quadrature bird-cage resonator at 298 K. T_1 values were determined using a saturation-recovery spin-echo sequence (TR values from 50 ms to 10 s) and T_2 values using a 64-echo Carl-Purcell-Meiboom-Gill (CPMG) sequence (TE values from 7.5 ms to 640 ms). Regions of interest (ROIs) were drawn on the first image of the image sequence and the intensity values extracted and fit to the following equations:

$$M_Z(t) = M_0(1 - e^{-TR/T_1})$$

$$M_{XY}(t) = M_0 e^{-TE/T_2}$$

Where Mz and Mxy are the signal intensities at time TR or TE, and M_0 is the signal intensity at equilibrium.

Cytotoxicity assays: HFF-1 cells were plated at a density of $1x10^4$ cells/well in a 96-well plate at 37ºC in 5% CO_2 atmosphere (200 µL per well, number of repetitions = 5). After 24 h of culture, the medium in the wells was replaced with fresh medium containing magnetic NPs in varying concentrations from 0.1 µg/mL to 100 µg/mL. After 24 h, the supernatant of each well was replaced by 200 µL of fresh medium with 3-[4,5-dimethylthiazol-2-yl]-2,5-diphenyl tetrazolium bromide (MTT) (0.5 mg/mL). After 2 h of incubation at 37ºC and 5% CO_2 the medium was removed and the formed formazan crystals were solubilized with 200 µL of DMSO, and the solution was vigorously mixed to dissolve the formed dye. Two controls were performed to evaluate the cytotoxicity: 1) as negative control, cells unexposed to NPs were used, and 2) as positive control, the cells were exposed to ethanol (20% v/v) for 15 min prior to the MTT procedure. The absorbance of each well was read on a microplate reader (Dynatech MR7000 instruments) at 550 nm. The relative cell viability (%) and its error

related to control wells containing cell culture medium without NPs were calculated by the following equations:

$$\boldsymbol{Relative\ Cell\ Viability}\ (\boldsymbol{RCV})\ (\%) = \frac{[\boldsymbol{Abs}]\boldsymbol{test} - [\boldsymbol{Abs}]\ \boldsymbol{Pos.Control}}{[\boldsymbol{Abs}]\ \boldsymbol{Neg.Control} - [\boldsymbol{Abs}]\ \boldsymbol{Pos.Control}} \times \mathbf{100}$$

$$\boldsymbol{Error}\ (\%) = \mathbf{RCVtest} \times \sqrt{\left(\frac{[\boldsymbol{\sigma}]\mathbf{test}}{[\mathbf{Abs}]\mathbf{test}}\right)^2 + \left(\frac{[\boldsymbol{\sigma}]\mathbf{control}}{[\mathbf{Abs}]\mathbf{control}}\right)^2}$$

where σ is the standard deviation.

Cell morphology studies: HFF-1 cells were plated at a density of $1x10^4$ cells/well in a 96-well plate at 37ºC in 5% CO_2 atmosphere (200 µL per well, number of repetitions = 5). After 24 h of culture, the medium in the wells was replaced with fresh medium containing the NPs in varying concentrations from 0.1 µg/mL to 100 µg/mL. As in the cytotoxicity assays, after 24 h, ethanol was added to the positive control wells. After 15 min, all the wells were stained with DAPI (4',6-Diamidino-2-phenylindole) (dilution 1:3000) to label nuclei in all cells, although with stronger labeling in live cells, and TO-PRO-3 Iodine to only label dead cells (dilution 1:1000). The cell morphology images were acquired using a Perkin Elmer Operetta High Content Imaging System with a 20x LWD 0.45 NA air objective lens. 5 well replicas for each condition were analyzed with 10 random image fields captured per well. For each field, fluorescence images for DAPI and TO-PRO-3, plus a bright field image were captured. Cell mortality percentages were calculated automatically by Operetta Harmony software, whereby all nuclei (dead and alive) were identified from the DAPI staining and the percentage of dead cells then determined by the number of nuclei also possessing high levels of TO-PRO-3 staining.

Statistical analysis: The statistical analysis was performed using the SPSS package (SPSS Inc., Chicago, Illinois). Cell viability is shown as mean ± standard deviation (SD). Student's t-test or two-way analysis of variance was used to determine significant

differences between different NPs or different experimental conditions. The level of significance was set at $p<0.05$.

Acknowledgements

Financial support was provided by the Spanish Ministry of Economy and Competitiveness (CTQ2017-86655-R to MPL and MLGM; CTQ2016-78580-C2-2-R to IFF) and by the VI PPIT of the University of Seville to MPL. MPL also thanks to the V Plan Propio of the University of Seville for the Postdoctoral Fellowship. Authors would like to thank the functional Characterization, Biological, Microanalysis and NMR services from CITIUS, and Dr. John R. Pearson for useful discussions in cell experiments.

Keywords: Magnetic Nanoparticles • Ligand Exchange • Catechol • Click Chemistry • MRI contrast agents

TOC

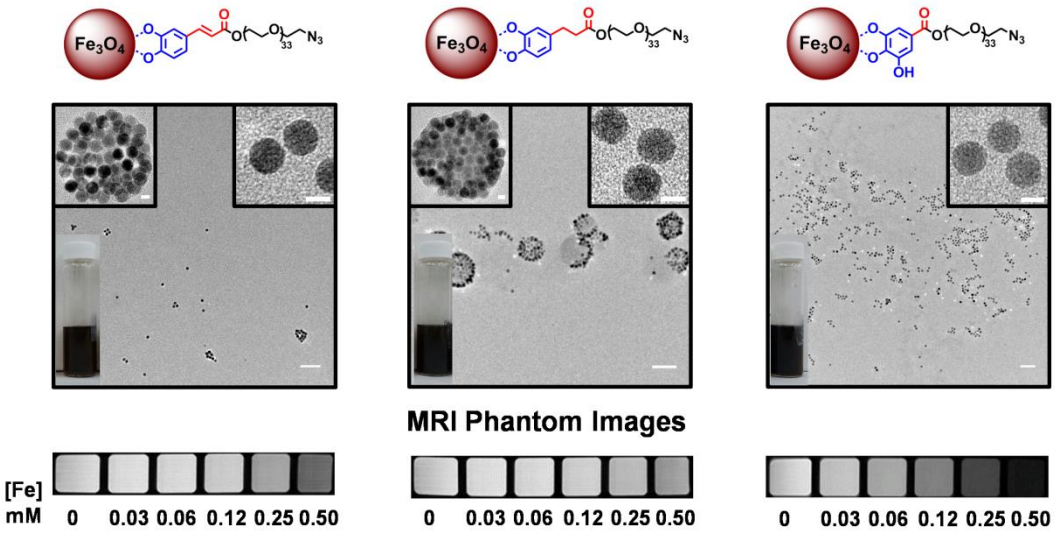

Clickable magnetic nanoparticles were prepared by a high-yield synthetic route. The synthetic design is based on a modular and versatile hetero bi-functional PEG spacer with an azide group and catechol anchor moieties with different stereo-electronic features. The azido functionalized nanoparticles exhibited excellent characteristics as T_2 MRI contrast agents with low cytotoxicity making them promising nanomedicine precursors.

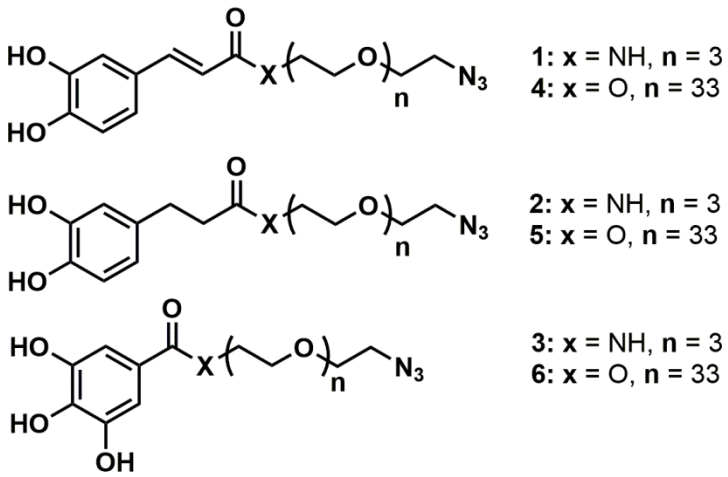

Figure 1. Catechol derived ligand structures.

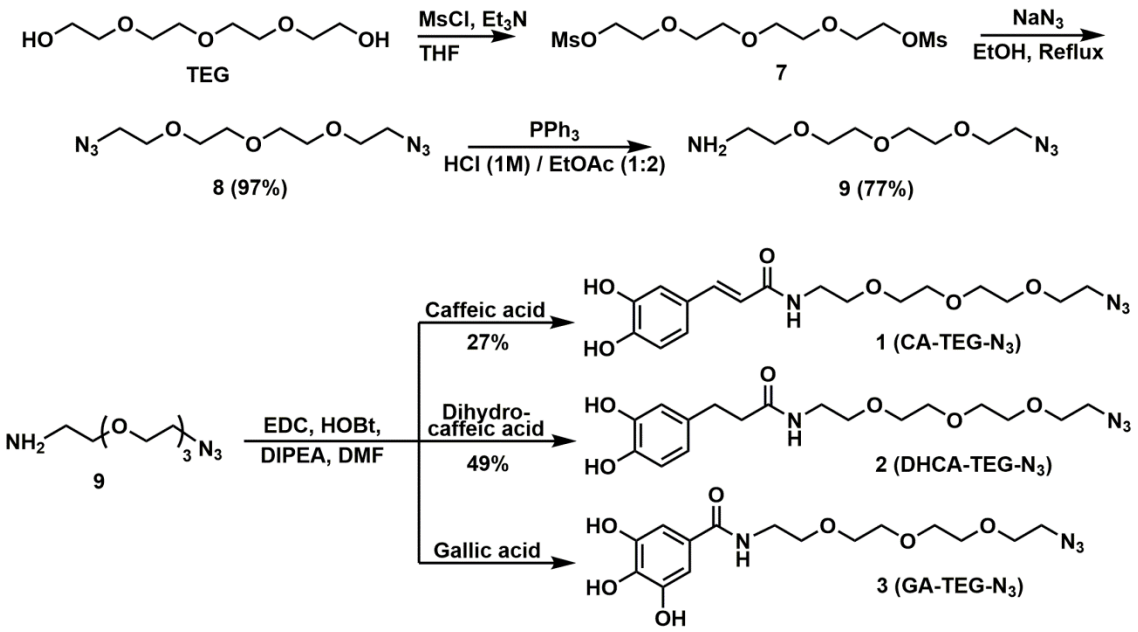

Scheme 1. Synthesis of catechol derived TEG-N_3 ligands (**1-3**).

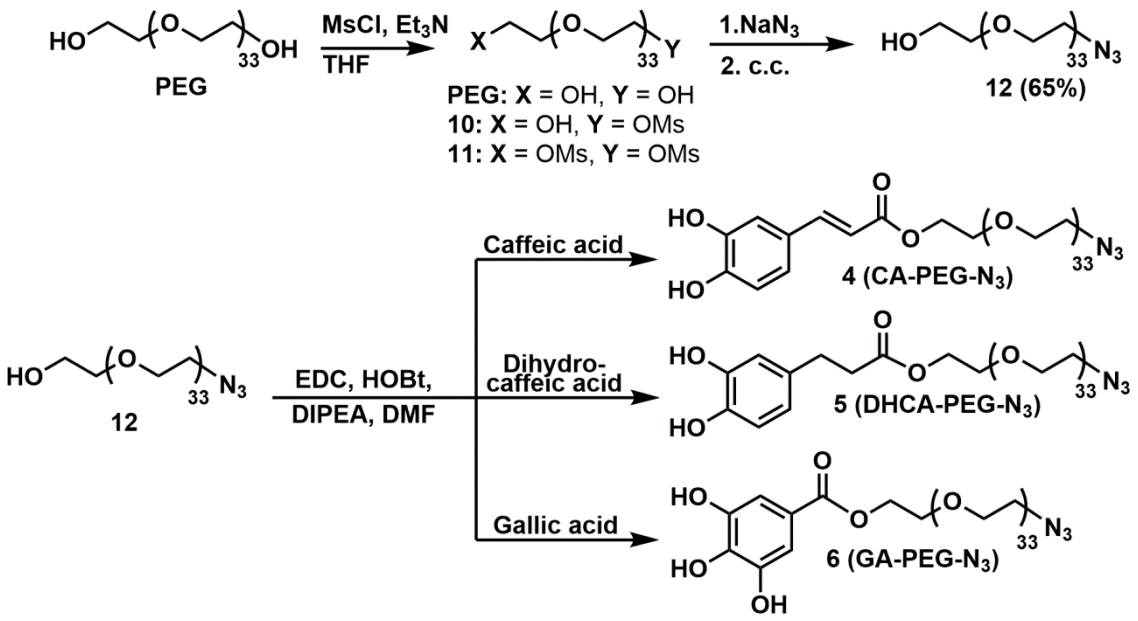

Scheme 2. Synthesis of catechol derived PEG-N_3 ligands (**4-6**).

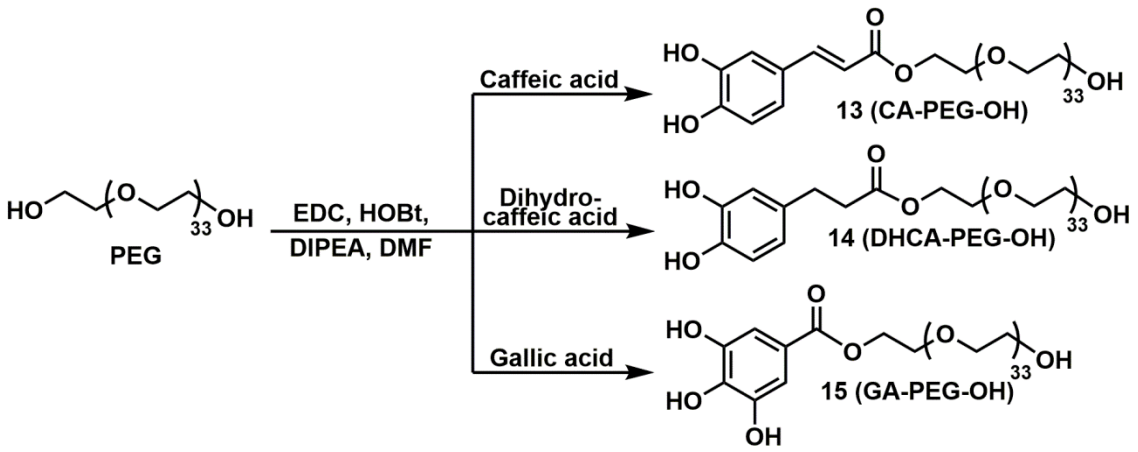

Scheme 3. Synthesis of catechol derived PEG-OH ligands (**13-15**).

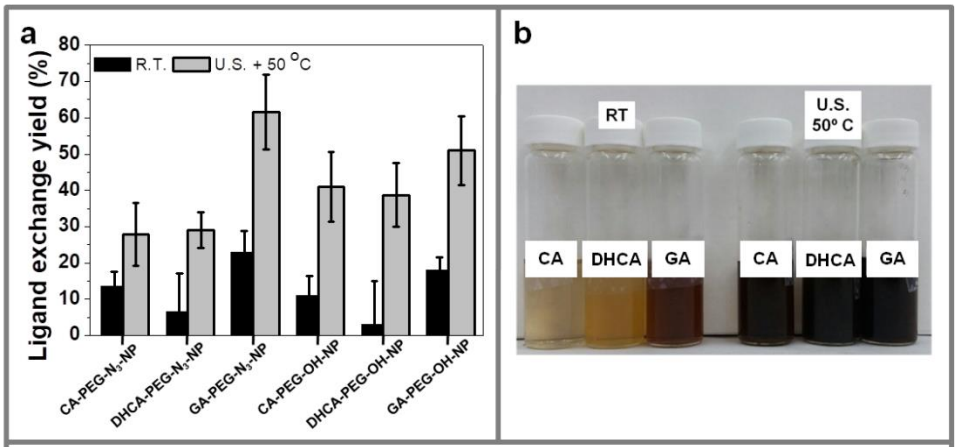

c

NP	Ligand exchange Yield (%)		HD sizes (nm)		
	r.t.	u.s.	water	PBS	FBS
CA-PEG-N_3	11	41	49.5	54.3	29.2
DHCA-PEG-N_3	3	38	67.8	94.3	51.5
GA-PEG-N_3	18	51	39.6	39.3	34.5
CA-PEG-OH	13.6	28	24.6	22.4	30.5
DHCA-PEG-OH	6.5	29	27.5	27.4	24.6
GA-PEG-OH	23	61	21.7	22.2	20

Figure 2. a) Ligand exchange yield of the two protocols quantified by ICP-MS by measuring the iron content before and after the procedure. b) Picture comparing the ligand exchange protocols using the PEG-OH derived ligands. c) Ligand exchange yield and HD sizes of the catechol derived NPs.

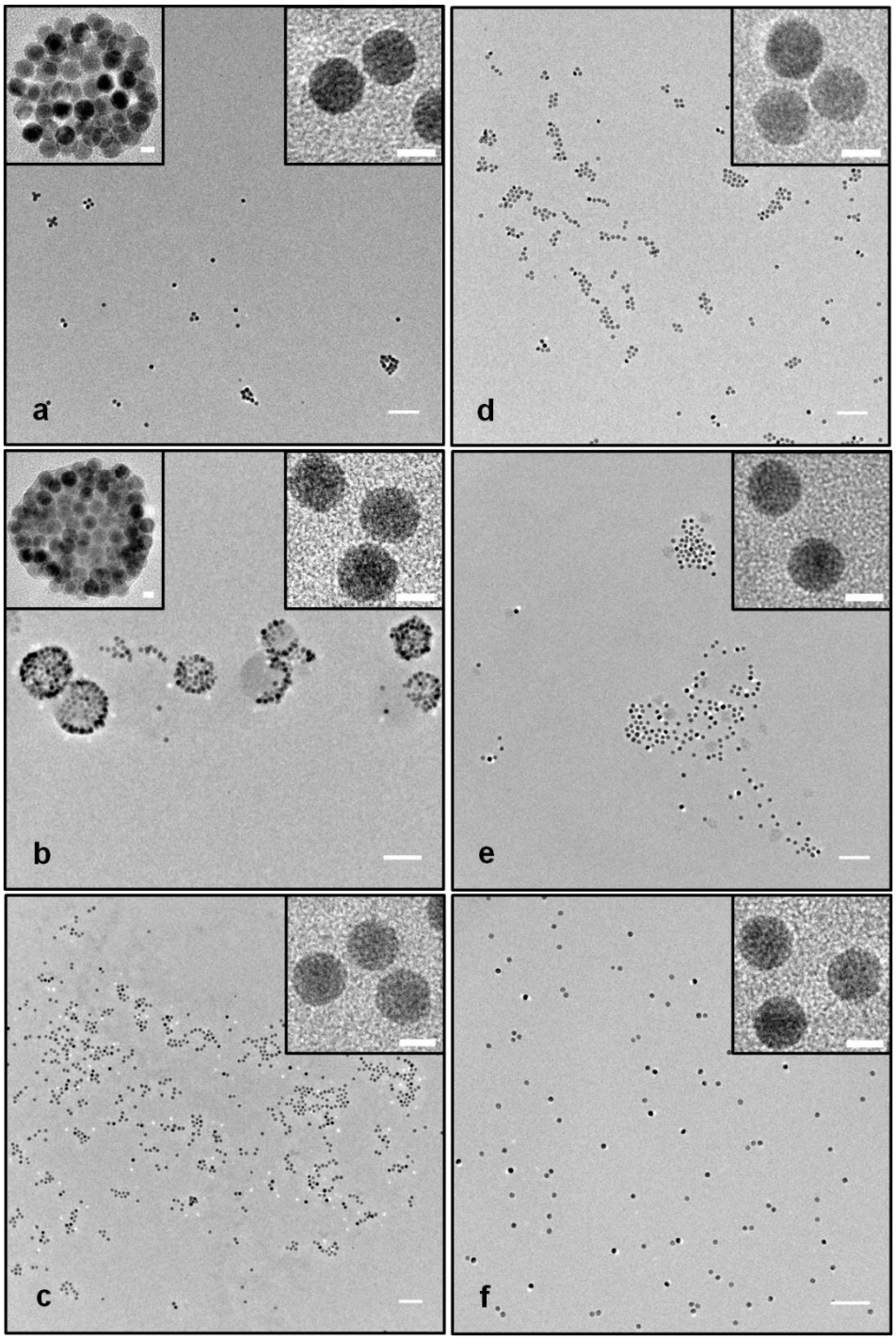

Figure 3. Representative TEM images of the funcionalized NPs with: a) CA-PEG-N_3, b) DHCA-PEG-N_3, c) GA-PEG-N_3, d) CA-PEG-OH, e) DHCA-PEG-OH and f) GA-PEG-OH, Scale bars correspond to 200 nm for low magnification TEM images and 10 nm for the insets.

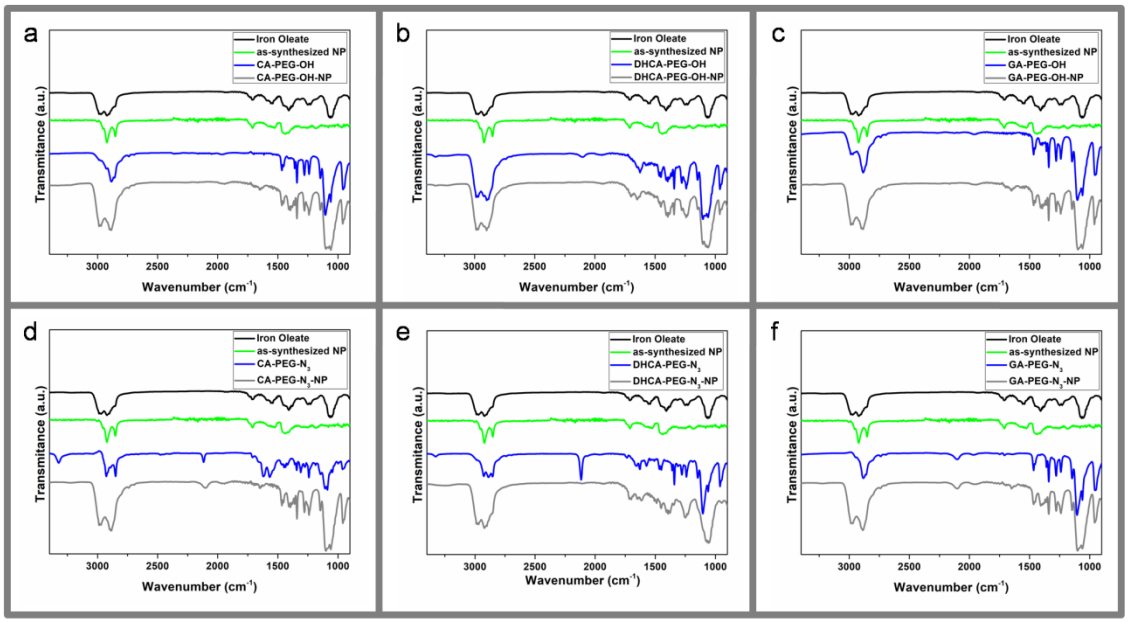

Figure 4. Comparison of the FTIR spectra: ligands (blue lines), functionalized NPs (grey lines), iron oleate precursor (black lines) and as-synthesized NPs (green lines).

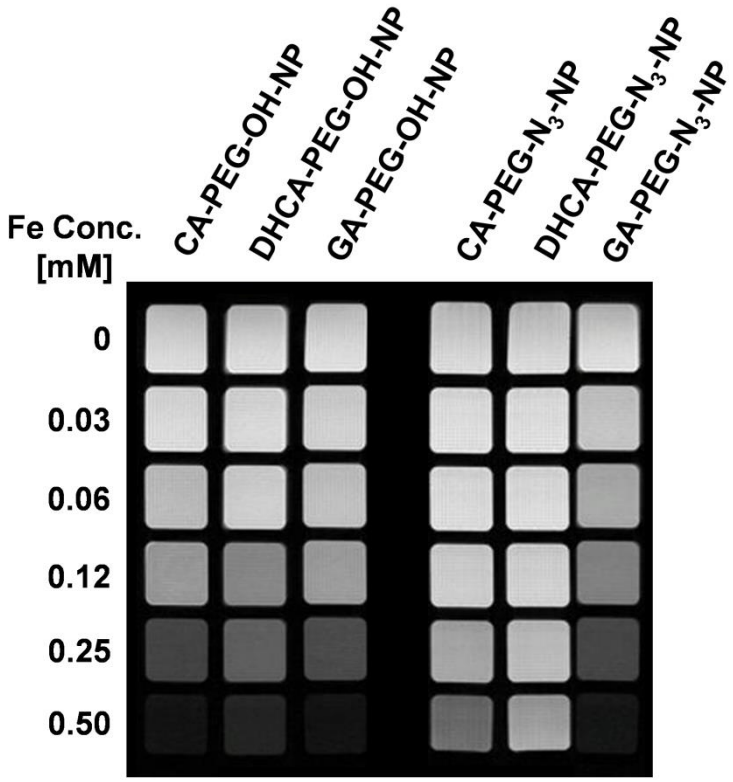

Figure 5. *In vitro* T_2 weighted MRI at 9.4 T of catechol functionalized NPs.

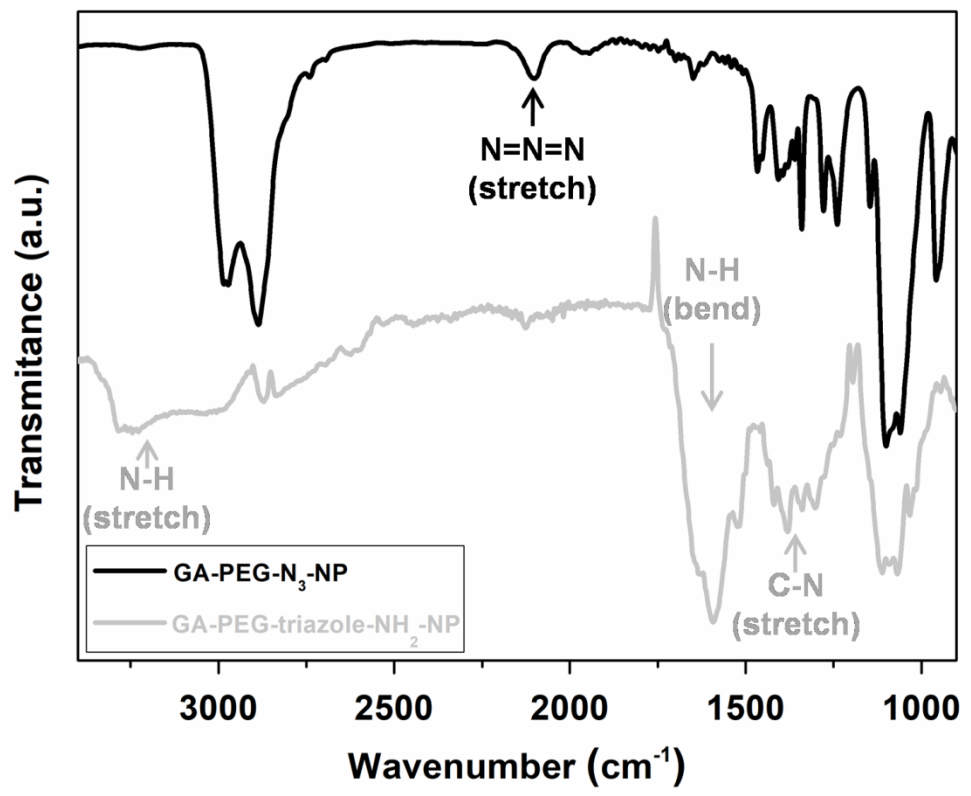

Figure 6. FTIR spectra of GA-PEG-N_3-NP before click reaction (black) and GA-PEG-triazole-NH_2-NP spectra after click reaction (grey).

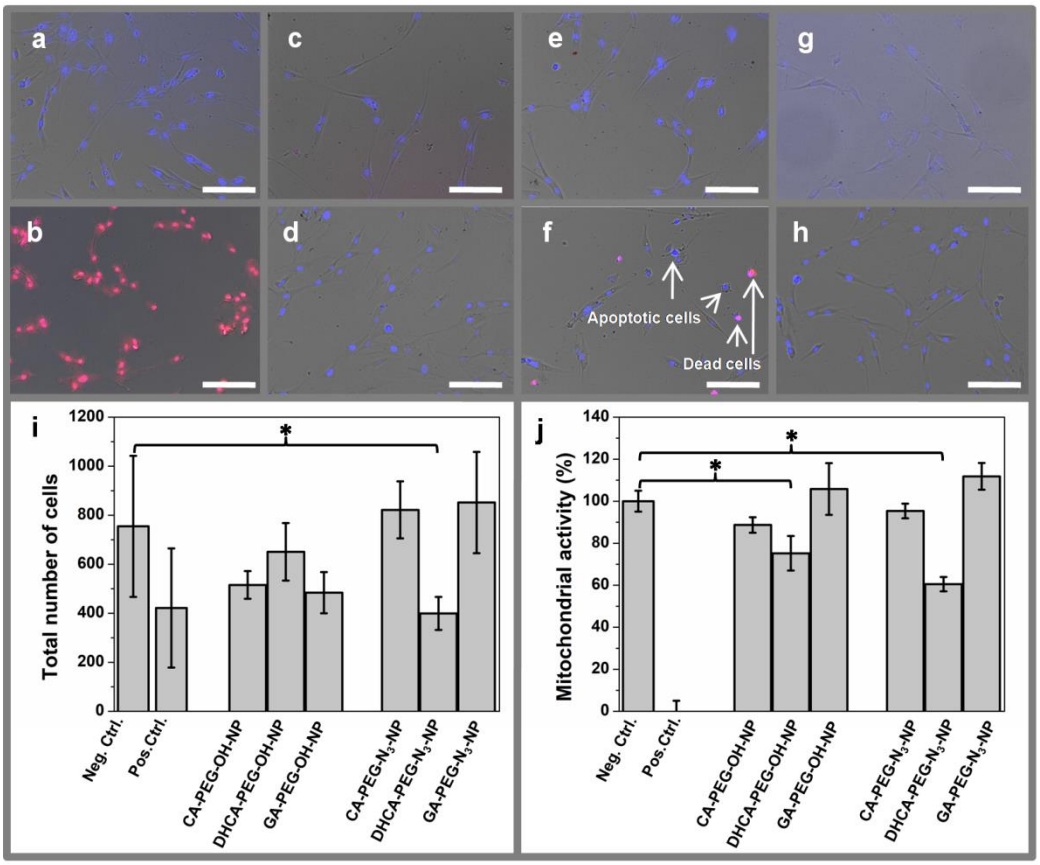

Figure 7. Live/dead viability assays on HFF-1 fibroblasts : a) Negative control, b) Positive control, cells exposed to 100 µg/mL of: c) CA-PEG-OH-NPs, d) CA-PEG-N_3-NPs, e) DHCA-PEG-OH-NPs, f) DHCA-PEG-N_3-NPs g) GA-PEG-OH-NPs, and h) GA-PEG-N_3-NPs. The images show the merge of bright field (grey), DAPI (blue) and TO-PRO-3 Iodine (red). Scale bar corresponds to 50 nm. i) Analysis of total number of cells per well exposed to 100 µg/mL of different NPs in live-dead assay ($p<0.05$). j) MTT assay of cells exposed to 100 µg/mL of NPs ($p<0.05$).

1. R. M. Dragoman, M. Grogg, M. I. Bodnarchuk, P. Tiefenboeck, D. Hilvert, D. N. Dirin and M. V. Kovalenko, *Chemistry of Materials*, 2017, 29, 9416-9428.

2. J. H. Lee, Y. M. Huh, Y. W. Jun, J. W. Seo, J. T. Jang, H. T. Song, S. Kim, E. J. Cho, H. G. Yoon, J. S. Suh and J. Cheon, *Nature Medicine*, 2007, 13, 95-99.

3. H. B. Na, I. C. Song and T. Hyeon, *Advanced Materials*, 2009, 21, 2133-2148.

4. H. B. Na, I. S. Lee, H. Seo, Y. I. Park, J. H. Lee, S. W. Kim and T. Hyeon, *Chemical Communications*, 2007, DOI: 10.1039/b712721a, 5167-5169.

5. W. Wei, X. Zhang, X. Chen, M. Zhou, R. Xu and X. Zhang, *Nanoscale*, 2016, 8, 8118-8125.

6. N. Zhu, H. Ji, P. Yu, J. Niu, M. U. Farooq, M. W. Akram, I. O. Udego, H. Li and X. Niu, *Nanomaterials*, 2018, 8.

7. M. Zhu, G. Nie, H. Meng, T. Xia, A. Nel and Y. Zhao, *Acc Chem Res*, 2013, 46, 622-631.

8. C. Caro, D. Egea-Benavente, R. Polvillo, J. L. Royo, M. Pernia Leal and M. L. García-Martín, *Colloids and Surfaces B: Biointerfaces*, 2019, 177, 253-259.

9. M. A. Boles, D. Ling, T. Hyeon and D. V. Talapin, *Nature materials*, 2016, 15, 141-153.

10. M. Pernia Leal, C. Caro and M. L. García-Martín, *Nanoscale*, 2017, 9, 8176-8184.

11. M. P. Leal, C. Muñoz-Hernández, C. C. Berry and M. L. García-Martín, *RSC Advances*, 2015, 5, 76883-76891.

12. Y. W. Jun, J. H. Lee and J. Cheon, *Angewandte Chemie - International Edition*, 2008, 47, 5122-5135.

13. C. Ghobril, G. Popa, A. Parat, C. Billotey, J. Taleb, P. Bonazza, S. Begin-Colin and D. Felder-Flesch, *Chemical Communications*, 2013, 49, 9158-9160.

14. M. Amiri, M. Salavati-Niasari and A. Akbari, *Advances in Colloid and Interface Science*, 2019, 265, 29-44.

15. D. Kim, K. Shin, S. G. Kwon and T. Hyeon, *Advanced Materials*, 2018, 30.

16. E. Amstad, T. Gillich, I. Bilecka, M. Textor and E. Reimhult, *Nano Letters*, 2009, 9, 4042-4048.

17. M. Pernia Leal, S. Rivera-Fernández, J. M. Franco, D. Pozo, J. M. De La Fuente and M. L. García-Martín, *Nanoscale*, 2015, 7, 2050-2059.

18. K. El-Boubbou, *Nanomedicine*, 2018, 13, 929-952.

19. K. Hola, Z. Markova, G. Zoppellaro, J. Tucek and R. Zboril, *Biotechnology advances*, 2015, 33, 1162-1176.

20. Y. Liu, T. Chen, C. Wu, L. Qiu, R. Hu, J. Li, S. Cansiz, L. Zhang, C. Cui, G. Zhu, M. You, T. Zhang and W. Tan, *Journal of the American Chemical Society*, 2014, 136, 12552-12555.

21. P. C. Liang, Y. C. Chen, C. F. Chiang, L. R. Mo, S. Y. Wei, W. Y. Hsieh and W. L. Lin, *International Journal of Nanomedicine*, 2016, 11, 2021-2037.

22. H. C. Kolb, M. G. Finn and K. B. Sharpless, *Angewandte Chemie - International Edition*, 2001, 40, 2004-2021.

23. M. A. White, J. A. Johnson, J. T. Koberstein and N. J. Turro, *Journal of the American Chemical Society*, 2006, 128, 11356-11357.

24. H. B. Na, G. Palui, J. T. Rosenberg, X. Ji, S. C. Grant and H. Mattoussi, *ACS Nano*, 2012, 6, 389-399.

25. J. Gallo, N. J. Long and E. O. Aboagye, *Chemical Society Reviews*, 2013, 42, 7816-7833.

26. M. P. Leal, M. Assali, I. Fernández and N. Khiar, *Chemistry - A European Journal*, 2011, 17, 1828-1836.

27. M. Colombo, S. Sommaruga, S. Mazzucchelli, L. Polito, P. Verderio, P. Galeffi, F. Corsi, P. Tortora and D. Prosperi, *Angewandte Chemie - International Edition*, 2012, 51, 496-499.

28. O. K. Arriortua, M. Insausti, L. Lezama, I. Gil de Muro, E. Garaio, J. M. de la Fuente, R. M. Fratila, M. P. Morales, R. Costa, M. Eceiza, M. Sagartzazu-Aizpurua and J. M. Aizpurua, *Colloids and Surfaces B: Biointerfaces*, 2018, 165, 315-324.

29. T. Lam, P. K. Avti, P. Pouliot, F. Maafi, J. C. Tardif, É. Rhéaume, F. Lesage and A. Kakkar, *Nanomaterials*, 2016, 6.

30. E. Amstad, M. Textor and E. Reimhult, *Nanoscale*, 2011, 3, 2819-2843.

31. A. K. L. Yuen, G. A. Hutton, A. F. Masters and T. Maschmeyer, *Dalton Transactions*, 2012, 41, 2545-2559.

32. H. Mattoussi, K. Susumu, H. T. Uyeda and I. L. Medintz, *Journal of Biomedicine and Biotechnology*, 2007, 2007.

33. N. Khiar, M. P. Leal, R. Baati, C. Ruhlmann, C. Mioskowski, P. Schultz and I. Fernández, *Chemical Communications*, 2009, DOI: 10.1039/b904717d, 4121-4123.

34. G. Lamanna, M. Kueny-Stotz, H. Mamlouk-Chaouachi, C. Ghobril, B. Basly, A. Bertin, I. Miladi, C. Billotey, G. Pourroy, S. Begin-Colin and D. Felder-Flesch, *Biomaterials*, 2011, 32, 8562-8573.

35. J. Hühn, C. Carrillo-Carrion, M. G. Soliman, C. Pfeiffer, D. Valdeperez, A. Masood, I. Chakraborty, L. Zhu, M. Gallego, Z. Yue, M. Carril, N. Feliu, A. Escudero, A. M. Alkilany, B. Pelaz, P. del Pino and W. J. Parak, *Chemistry of Materials*, 2017, 29, 399-461.

36. B. Pelaz, P. Del Pino, P. Maffre, R. Hartmann, M. Gallego, S. Rivera-Fernández, J. M. De La Fuente, G. U. Nienhaus and W. J. Parak, *ACS Nano*, 2015, 9, 6996-7008.

37. U. O. Häfeli, J. S. Riffle, L. Harris-Shekhawat, A. Carmichael-Baranauskas, F. Mark, J. P. Dailey and D. Bardenstein, *Molecular Pharmaceutics*, 2009, 6, 1417-1428.

38. R. M. Patil, N. D. Thorat, P. B. Shete, P. A. Bedge, S. Gavde, M. G. Joshi, S. A. M. Tofail and R. A. Bohara, *Biochemistry and Biophysics Reports*, 2018, 13, 63-72.

39. Q. Feng, Y. Liu, J. Huang, K. Chen, J. Huang and K. Xiao, *Scientific reports*, 2018, 8.

40. O. I. Aruoma, A. Murcia, J. Butler and B. Halliwell, *Journal of Agricultural and Food Chemistry*, 1993, 41, 1880-1885.

41. C. A. Gomes, T. G. Girão Da Cruz, J. L. Andrade, N. Milhazes, F. Borges and M. P. M. Marques, *Journal of Medicinal Chemistry*, 2003, 46, 5395-5401.